Mon. Not. R. Astron. Soc. **000**, 1–8 (2014) Printed 6 May 2014 (MN LATEX style file v2.2)

Prospects of 3D mapping of the Galactic Centre clouds with X-ray polarimetry

F. Marin[1⋆], V. Karas[1], D. Kunneriath[1] and F. Muleri[2]
[1]*Astronomical Institute of the Academy of Sciences, Boční II 1401, CZ-14100 Prague, Czech Republic*
[2]*INAF/IAPS, Via del Fosso del Cavaliere 100, I-00133 Roma, Italy*

arXiv:1405.0898v1 [astro-ph.GA] 5 May 2014

Accepted 2014 April 10. Received 2014 March 27; in original form 2014 February 20

ABSTRACT

Despite past panchromatic observations of the innermost part of the Milky Way, the overall structure of the Galactic Centre (GC) remains enigmatic in terms of geometry. In this paper, we aim to show how polarimetry can probe the three-dimensional position of the molecular material in the central ∼100 pc of the GC. We investigate a model where the central supermassive black hole Sgr A* is radiatively coupled to a fragmented circumnuclear disc (CND), an elliptical twisted ring representative of the central molecular zone (CMZ), and the two main, bright molecular clouds Sgr B2 and Sgr C. 8 – 35 keV integrated polarization mapping reveals that Sgr B2 and Sgr C, situated at the two sides of the CMZ, present the highest polarization degrees (66.5 and 47.8 per cent respectively), both associated with a polarization position angle $\psi = 90°$ (normal to the scattering plane). The CND shows a lower polarization degree, 1.0 per cent with ψ = -20.5°, tracing the inclination of the CND with respect to the Galactic plane. The CMZ polarization is spatially variable. We also consider a range of spatial locations for Sgr A* and the reprocessing media, and investigate how the modeled three-dimensional geometry influences the resulting GC polarization. The two reflection nebulae are found to always produce high polarization degrees ($\gg$ 10 per cent). We show that a 500 ks observation with a broadband polarimeter could constrain the location and the morphology of the scattering material with respect to the emitting source, revealing the past activity of Sgr A*.

Key words: polarization – radiative transfer – scattering – Galaxy: centre – Galaxy: nucleus – X-rays: general.

1 INTRODUCTION

Situated at a distance of ∼ 8 kpc, the central region of our Galaxy hosts Sgr A*, the closest-to-Earth supermassive, 4.3×10^6 $M_\odot$, black hole (Ghez et al. 2008; Gillessen et al. 2009). Around the potential well of Sgr A* is a concentration of active star formation sites and gigantic molecular clouds (Yusef-Zadeh et al. 2008, 2009) that makes the Galactic Centre (GC) of the Milky Way an excellent site for testing theories against observations in the context of an accreting black hole. It appears, however, that the present accretion rate of Sgr A* is extremely small, about 10^{-8} $M_\odot.y^{-1}$ near the event horizon (Baganoff et al. 2003), so the X-ray luminosity is only about $L_X \sim 2 \times 10^{33}$ ergs.s^{-1} (Baganoff et al. 2001; Quataert 2002).

Such quiescence is in disagreement with past X-ray observations of the Eastern massive molecular cloud Sgr B2 that revealed a very steep spectrum with a strong emission line at 6.4 keV related to iron fluorescence, suggesting that part of the diffuse emission of Sgr B2 is due to reprocessing (Sunyaev et al. 1993; Koyama et al. 1996). The lack of nearby X-ray sources, bright enough to account for the spectrum of Sgr B2, lead Sunyaev et al. (1993) to classify Sgr B2 as a reflection nebula, shining the reprocessed emission from a past Sgr A* outburst ($L_X > 10^{39}$ erg.s^{-1}). From geometrical considerations, Sunyaev & Churazov (1998) and Murakami et al. (2000) postulated that Sgr A* underwent a flaring period that illuminated the reflection nebula, a hypothesis consolidated by the discovery of a similar behavior in the Western Sgr C complex (Murakami et al. 2001). From a long-term time variability study, Inui et al. (2009) inferred that the outburst happened ∼ 300 years ago, a conclusion shared by Ponti et al. (2010) who found that Sgr A* was active ∼ 400 years ago and again about 100 years ago. The estimated duration of the flare depends on the spatial location of the reflector which, unfortunately, cannot be properly constrained using X-ray spectroscopy or timing analyzes.

To overcome this difficulty, Churazov et al. (2002) pro-

⋆ E-mail: frederic.marin@asu.cas.cz

posed X-ray polarization as a mechanism to: 1) probe the flaring theory as the resulting, reprocessed X-ray should be polarized and 2) estimate the three-dimensional location of the clouds. Using a single cloud of radius 10 pc, with Thomson optical depth of 0.5 and filled with neutral, solar abundance matter, they show that the reflected radiation should be highly polarized ($>$ 30 per cent) with a direction of polarization normal to the scattering plane. Using a simple model, Churazov et al. (2002) proved that any detection of polarized X-ray emission from the reflection nebulae around Sgr A* would bring constraints on the morphology and position of the scattering clouds, the duration of the flare and the location of the illuminating region. Yet, to be compared with future X-ray polarimetric observations, GC modeling needs further refinement. In particular, radiative coupling between the reflection nebulae and multiple scattering must be taken into account for time-delay, particularly in the case of short duration flares (Sunyaev & Churazov 1998; Churazov et al. 2002). Moreover, the dense and warm environment around the central few parsecs around Sgr A* is likely to alter the polarization vector of radiation reaching the molecular clouds. The presence of the most massive component of the central molecular zone along the Galactic plane (sometimes referred as the "disc population", Heiligman 1987; Bally et al. 1988), forming dust lanes along the observer's line-of-sight, is an additional component to the system that can alter polarization results by absorption and reprocessing.

Intending to provide a more accurate estimation of the X-ray polarization signal that can emerge from multiple scattering, absorption and dilution from the source, we build a $2^\circ \times 2^\circ$ ($\sim 288 \times 288$ pc; at 8.5 kpc $1'' \approx 0.04$ pc) model of the GC in Sect. 2.1. We analyze the resulting 8 – 35 keV polarization map in Sect. 2.2, estimating both integrated and localized polarized X-ray emission. We extend the morphological parameterization in order to explore the influence of the location of the reprocessing components onto polarization in Sect. 2.3 and investigate the polarization detectability of Sgr B2 and Sgr C in Sect. 2.4. We discuss our work and draw conclusions in the last sections of this paper.

2 POLARIZED EMISSION FROM THE GALACTIC CENTRE

The complex emitting and scattering environment of Sgr A* remains enigmatic in terms of morphology. Constraints on the central hundred parsecs derived by spectroscopy and velocity measurement in the radio (e.g. Tsuboi et al. 1999), infrared (e.g. Molinari et al. 2010) and X-ray/soft-γ domains (e.g. Sunyaev et al. 1991) helped to estimate the three-dimensional gas distribution. Using the geometrical constraints obtained so far, we now investigate the resulting polarization signatures from the GC using X-ray polarimetry. Knowing that past X-ray observations (Koyama et al. 1986, 1989; Sidoli & Mereghetti 1999) have revealed the presence of a diffuse plasma emission toward the GC that could dilute the polarization signal below 7 keV (Mewe 1999; Liedahl 1999), we limit the investigation to the soft X-ray band. We center our analysis in the 8 – 35 keV energy domain to: 1) avoid most of the dilution by the GC plasma emission, 2) avoid local polarization dilution by the unpolarized 6.4 keV iron emission line and 7.1 keV edge structure (Murakami et al. 2000), and 3) extend the 2 – 8 keV simulations achieved by Churazov et al. (2002).

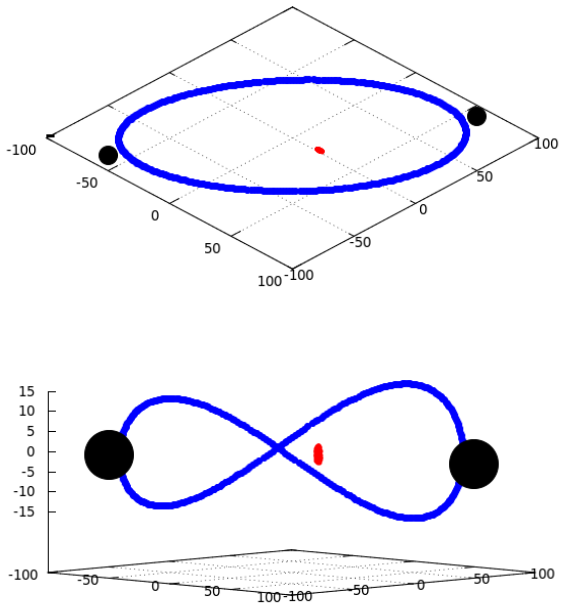

Figure 1. Sketch of the three-dimensional GC structure. The 100 pc elliptical twisted ring (Molinari et al. 2011) is drawn in blue, the fragmented circumnuclear disc surrounding Sgr A* in red, and Sgr B2 (left, Eastern cloud) and Sgr C (right, Western cloud) in black. Axes are in parsec units and the sketch is roughly to scale. *Top*: pole-on view of the GC; *bottom*: edge-on (observed) view of the GC.

2.1 Modeling X-ray polarization from the inner 100 pc

Polarization modeling was achieved using STOKES (Goosmann & Gaskell 2007; Marin et al. 2012a), a Monte Carlo code that takes into account the polarized component of light. STOKES performs three-dimensional radiative transfer simulations within various geometries of reprocessing regions. Originally developed for optical/UV investigation, the code was extended to the X-ray range with the inclusion of inelastic scattering responsible for the Compton hump above 10 – 20 keV, absorption, photo-ionisation and recombination effects. Detailed information about STOKES calculation of X-ray polarization are given in Goosmann (2010).

In the context of the GC, unpolarized input photons are generated from a point-like, isotropic source that emits 8 – 35 keV photons according to a power-law spectral energy distribution $F_* \propto \nu^{-\alpha}$. The spectral index α is fixed to unity in order to match the photon index of Sgr A* flaring events (~ 2, Porquet et al. 2003; Baganoff et al. 2003; Bélanger et al. 2005; Neilsen et al. 2013; Barrière et al. 2014) that can be representative of the past activity of the supermassive black hole. Finally, the source is displaced by ~ 22 pc in projection from the center of the model toward the Western galactic longitude to be consistent with the shifted gas dis-

tribution within the central molecular zone (CMZ, Molinari et al. 2011).

In our model (a sketch is presented in Fig. 1.) the inner 5 pc around Sgr A* is surrounded by a clumpy distribution of 100 molecular gas spheres filled with cosmic abundance matter (hydrogen, helium, carbon, nitrogen, oxygen, neon, magnesium, silicate, sulfur and iron). The gas clouds, representative of the circumnuclear disc (CND), are arranged in a configuration similar to a fragmented disc tilted by 20° with respect to the Galactic plane (Ponti et al. 2013; Liu et al. 2014). The clumps have an hydrogen column density $> 10^{25}$ atom.cm^{-2} and an orbital velocity of 100 km.s^{-1} (Christopher et al. 2005); the gas temperature is fixed to 200 K (Mills et al. 2013).

At larger distances from Sgr A* and the CND, we implement a cold, dusty structure as proposed by Molinari et al. (2011). In their picture, a continuous chain of irregular clumps forms the CMZ in the shape of an elliptical twisted ring of molecular material. The ∞-shaped ring is parameterized according to Molinari et al. (2011)[1]. The resulting CMZ is composed of 300 spherical clouds with hydrogen column density 10^{24} atom.cm^{-2} (Ponti et al. 2013), gas temperature 80 K (Morris et al. 1983) and orbital velocity 80 km.s^{-1} (Molinari et al. 2011; Ponti et al. 2013). On the plane-of-the-sky, the ∞-shaped ring extends up to $\sim$ 100 pc in longitude and $\sim$ 25 pc in latitude.

We include into our model the two bright, complex reflection nebulae Sgr B2 and Sgr C. Located in the Eastern CMZ, Sgr B2 is the largest and heaviest molecular cloud within the inner 100 parsecs around Sgr A* (Murakami et al. 2001) and thus a prime target for scattering induced polarization. Sgr C is a complex structure composed of, at least, three separate components distant from each other, and holds the largest star forming region in the Western CMZ (Kendrew et al. 2013). Sgr B2 and Sgr C are located at the two extrema of the twisted elliptical ring and, according to the dependence on the cosine square of Thomson scattering, are likely to be the best targets for future X-ray polarimetric measurement. Sgr B2 is defined as a spherical cloud with an overall radius 7 pc, hydrogen column density 8×10^{23} atom.cm^{-2} and orbital velocity 60 km.s^{-1} (Ponti et al. 2010). Sgr C has an overall radius of 5 pc (Ryu et al. 2013), a hydrogen column density equals to 8×10^{22} atom.cm^{-2} (Kendrew et al. 2013) and we fix its orbital velocity to 60 km.s^{-1} (similar to Sgr B2). Both clouds are filled with neutral, cosmic abundance matter and are situated at $\sim$ 100 pc from the center of the model. However, from very-long-baseline interferometry (VLBI) and very long baseline array (VLBA) trigonometric parallax arguments, Reid et al. (2009) situate Sgr B2 in the front of the Galactic plane. To investigate the importance of the position of the scattering nebulae, we thus shift Sgr B2 by $\sim$ 10 pc toward the observer while Sgr C remains closer to the Western extrema.

Polarization being sensitive to any departure from symmetry, the combination of the structure proposed by Molinari et al. (2011), the off-center irradiating source, and the spatial shift of Sgr B2 (and to a lesser extent the one of Sgr C) are expected to enhance the production of spatially localized polarization.

[1] The original formula by Molinari et al. (2011) contains a typo. One must read $z = z_0 \sin\nu_{\rm orb}(\theta_t - \theta_z)$ instead of $z = z_0 \sin\nu_{\rm orb}(\theta_p - \theta_z)$, with the definitions of $z, z_0, \nu_{\rm orb}, \theta_t, \theta_p$ and θ_z to be found in Sect. 3.1 of their paper.

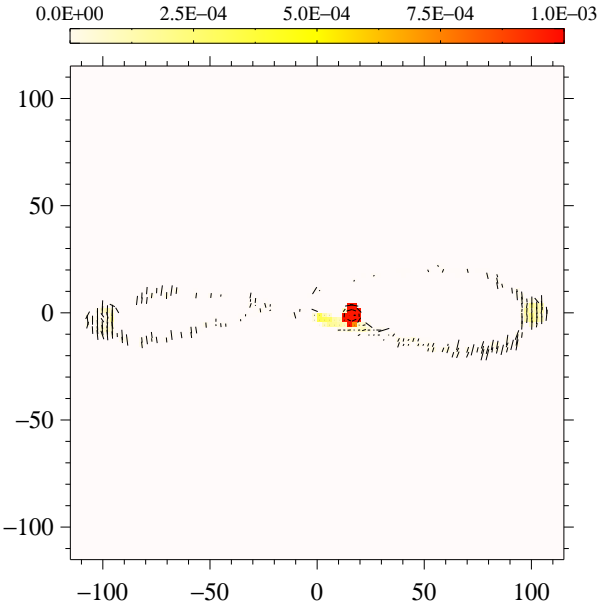

Figure 2. Integrated 8 – 35 keV model image of the polarized flux, PF/F_*, for the 2° × 2° region around the GC. PF/F_* is color-coded, with the color scale shown on top of the image (in arbitrary units). P and ψ are represented by black bars drawn in the center of each spatial bin. A vertical bar indicates a polarization angle of $\psi = 90°$ and a horizontal bar stands for an angle of $\psi = 0°$. The length of the bar is proportional to P.

2.2 Polarization results

We sampled a total of 10^9 photons and present in Fig. 2 an integrated, 8 – 35 keV, polarization map of the GC. The spatial resolution is set to 100 × 100 bins for the longitudinal and latitudinal axes, so that the photon flux is divided into 10^4 pixels. Each of these pixels is labeled by the position offset in parsecs and stores the four Stokes parameters of the 8 – 35 keV photons. The resulting polarized flux (PF/F_*, i.e. intensity times polarization degree) is normalized to the central flux F_* that is emitted into the same viewing direction, and is color-coded. The polarization degree P, ranging from 0 per cent (unpolarized) to 100 per cent (fully polarized), and the polarization position angle ψ are represented by black bars drawn in the center of each spatial bin. A vertical bar indicates a polarization position angle $\psi = 90°$ (perpendicular to the projected vertical axis of the model) and a horizontal bar stands for an angle $\psi = 0°$ (parallel to the projected vertical axis). The length of the bar is proportional to P.

The polarized flux, PF/F_*, traces the overall shape of the GC, emphasizing the ∞-shaped CMZ. PF/F_* reaches a maximum at the location of the CND surrounding Sgr A*, where the combination of the flux from the emitting source and the polarization of reprocessed photons by neutral material increases the polarized flux. However, the local polar-

Region	P [%]	ψ [°]
GC (integrated)	0.9	-22.8
CND	1.0	-20.5
Sgr B2	66.5	88.1
Sgr C	47.8	89.5

Table 1. Estimated 8 – 35 keV polarization degree P and polarization angle ψ of the 2° × 2° GC and individual reprocessing regions. Polarization angles are defined with respect to the projected vertical axis of the system.

ization degree is rather low, ∼ 1.0 per cent, when integrated over the CND (see Tab. 1). This is due to the disc-like geometry of the scattering material that is seen nearly pole-on by the observer. Thomson scattering-induced polarization being small for forward and backward scattering, the morphology of the CND thus favors low P. Increasing the filling factor of the CND or replacing it by a uniform disc has very little impact on P. The polarization position angle associated with the CND is not null (ψ = -20.5°) as the system is inclined by 20° with respect to the Galactic plane (Ponti et al. 2013).

Sgr B2 and Sgr C show the secondary, brightest polarized flux knots of the map. Polarization by electron scattering being the most efficient for orthogonal scattering angles, we find P = 66.5 per cent for Sgr B2 and P = 47.8 per cent for Sgr C. The difference in P is due to the spatial location of the cloud with respect to Sgr A* and the resulting asymmetry produced by this setup. Both the clouds present a polarization position angle roughly perpendicular to the vertical axis of the model, as predicted by Churazov et al. (2002). By measuring the angle between the emitting source, the cloud and the observer, X-ray polarimetry could properly reconstruct the position of the primary emitting source.

The CMZ polarization traces the shape of the structure, with partial disappearance of P due to low polarization degrees induced by forward and backward scattering, and dilution from unpolarized radiation from the source. P varies for each CMZ cloud and reaches a maximum for the Eastern and Western apoapse sections of the elliptical twisted ring, where the CMZ mixes with the giant molecular clouds. It is most likely that a large fraction of the ∞-shaped ring will be diluted by background, unpolarized emission from both plasma emission and Sgr A*, and thus be undetectable.

Finally, when integrating the whole 2° × 2° GC polarized emission, the model produces a net polarization degree of 0.9 per cent associated with a polarization position angle of -22.8°. The combined emission from Sgr A* and the CND thus dominates the whole polarization picture.

2.3 Impact of the location of components

Despite constraints brought by multi-wavelength observations (e.g. Eckart et al. 2008; Law et al. 2008), the GC remains puzzling in terms of gas morphology, composition and location. The three-dimensional parameterization modeled in Sect. 2.2 mainly relies on projected radial distances with respect to the Galactic plane. As noted by Reid et al. (2009), the actual location of the reflecting nebulae can be shifted from this plane but still conserve the same radial

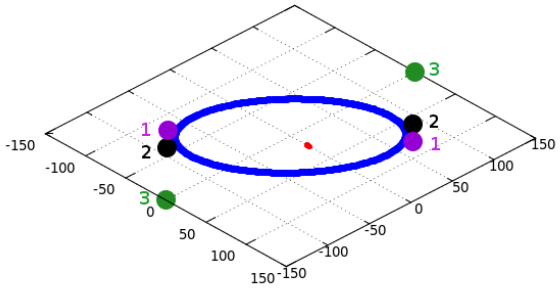

Figure 3. Investigating different locations of Sgr B2 and Sgr C that produce the same projected distances on the Galactic plane. The sketch is roughly to scale. *Legend*: clouds situated on the Galactic plane are shown in violet, clouds at the distances fixed in Sect. 2.1 in black and clouds situated at ∼ 100 pc from the Galactic plane in green. The same colors are used in Tab. 2 to identify P and ψ for each case.

projections. Polarimetry being sensitive to the geometry of the scattering system, we now depart from the assumed GC parameters listed in Sect 2.1 and test different locations of Sgr B2, Sgr C and Sgr A* (coupled to the CND).

We first explore the impact of different locations of Sgr B2 and Sgr C with respect to the Galactic plane, conserving a projected distance similar to the one derived by Molinari et al. (2011). For an observer situated on Earth, the three models summarized in Fig. 3 (seen from the pole) produce the same edge-on GC image. Similarly to our previous investigation, we spatially integrate the 8 – 35 keV net polarization of the three main scattering regions (CND, Sgr B2 and Sgr C) and we also evaluate the resulting polarization from the whole 2° × 2° GC in Tab. 2. The first model, with violet clouds, reproduces the extreme case where the two reflection nebulae lie at the apoapsis of the elliptical twisted ring of gas. As the scattering angle between the source, the reprocessing material and the observer is nearly orthogonal, P is maximum: 71.0 per cent for Sgr B2 and 64.0 per cent for Sgr C, both associated with a polarization position angle of ∼ 90°. When the reflection nebulae depart from the Galactic plane, P decreases as the scattering angle becomes narrower. For distant, ∼ 100 pc, scattering clouds (represented in green), P equals to 38.6 per cent for Sgr B2 and 16.0 per cent for Sgr C, with ψ remaining constant. The spatial location of Sgr B2 and Sgr C can thus be estimated from a measurement of the net polarization degree, as P decreases with the distance of the clouds from the Galactic plane. Independently of the position of the reflecting nebulae, $P_{\rm CND}$ and $\psi_{\rm CND}$ remain constant for the three models, still dominating the integrated GC picture despite the large amount of polarization produced by the scattering nebulae when the clouds are on the Galactic plane.

We then investigate the impact of the location of the central supermassive black hole and its surrounding CND on the total GC polarization. In Fig. 4, we show three possible locations of Sgr A*, paired with the CND, which give a projected distance of ∼ 0 pc from the center of the model (in brown), ∼ 22 pc (in red, such as in Sect. 2.1) and ∼ 42 pc.

Region	P [%]			ψ [°]		
	M_1	M_2	M_3	M_1	M_2	M_3
GC	0.9	0.9	1.0	-22.0	-22.8	-21.4
CND	1.0	1.0	1.0	-18.7	-20.5	-19.9
Sgr B2	71.0	66.5	38.6	91.5	89.1	91.3
Sgr C	64.0	47.8	16.0	90.4	89.5	89.6

Table 2. Estimated 8 – 35 keV polarization degree P and polarization angle ψ of the integrated 2° × 2° and individual reprocessing regions. $M_{1,2,3}$ and the colors refer to the three different radial positions of the colouds presented in Fig 3.

Region	P [%]			ψ [°]		
	M_4	M_5	M_6	M_4	M_5	M_6
GC	0.7	0.9	0.9	-39.8	-23.4	-21.8
CND	0.7	1.0	0.9	-36.0	-21.3	-20.3
Sgr B2	58.6	67.0	73.8	90.0	89.0	89.0
Sgr C	53.0	44.5	37.3	93.0	88.0	91.7

Table 3. Estimated 8 – 35 keV polarization degree P and polarization angle ψ of the integrated 2° × 2° and individual reprocessing regions. $M_{4,5,6}$ and the colors refer to the three different projected distances of Sgr A* / CND presented in Fig 4.

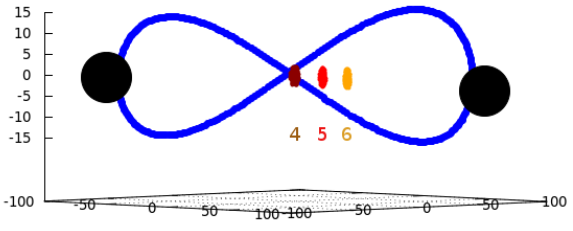

Figure 4. Investigating different projected distances for Sgr A* / CND on the Galactic plane. The sketch is roughly to scale. *Legend*: ∼ 0 pc projected distance from the center of the ∞-shaped ring in brown, distance fixed in Sect. 2.1 (∼ 22 pc) in red and ∼ 42 pc projected distance in orange. The same colors are used in Tab. 3 to identify P and ψ for each case.

Results for the 8 – 35 keV integrated polarization are given in Tab. 3. Independent of the position of Sgr A*, the surrounding cloudlet distribution that forms the CND produces a constant ∼ 1.0 per cent polarization degree since the composition and morphology of the CND enclosing Sgr A* did not vary. However, the polarization position angle differs between the model where the emitting source is situated at the center of the structure and models with shifted locations of Sgr A*. The difference is due to the ∞-shaped CMZ dust lane at the forefront of model, partially covering the central supermassive black hole in the first scenario. To reach the observer, radiation has to pass through this molecular strip, undergoing scattering events that alter its polarization position angle and marginally diminish the net polarization degree due to extra absorption. Similarly to Fig. 2 and Fig. 3, the integrated GC polarization is dominated by the reprocessed emission from the Sgr A* / CND duo. $P_{\rm Sgr\ B2}$ and $P_{\rm Sgr\ C}$ also show variations related to the location of the emitting source. While the polarization degree of $P_{\rm Sgr\ B2}$ increases with the (projected) departure of the emitting source from the center of the model, $P_{\rm Sgr\ C}$ diminishes. The source of unpolarized photons getting closer to $P_{\rm Sgr\ C}$, it enhances the local dilution of polarization and thus reduces the net Western P. The opposite effect occurs on the Eastern side of the model. The resulting polarization is still high (> 35 per cent) and both the reflection nebulae produce a perpendicular polarization position angle, since the Sgr A* / CND duo moved along the Galactic longitude only.

2.4 Detectability with available technology

The technology enabling the measurement of celestial X-ray polarization has greatly evolved since the 1970s, when the *8th Orbiting Solar Observatory* (*OSO-8*) carried the last flying non-solar X-ray polarimeter (Weisskopf et al. 1978). The new generation of Gas Pixel Detector (GPD), based on the photoelectric effect (Costa et al. 2001), overcomes the sensitivity limits of past X-ray polarimeters based on graphite-crystal Bragg diffraction at 45° or Thomson/Compton scattering, and is thus a new and technologically-ready instrument to probe the GC (Tagliaferri et al. 2012a; Soffitta et al. 2013).

Results from Sect. 2.2 and 2.3 showed that Sgr B2 and Sgr C are prime candidates for polarization observations as they are expected to produce a significant amount of polarization (≫ 10 per cent). Hence, to strengthen the case of X-ray polarimetry for the future of X-ray astronomy, we now investigate their detectability by exploring the minimum detectable polarization (MDP) that a past X-ray polarimetric project could have reached if it had been selected for launch. We focus on *NHXM*, the *New Hard X-ray Mission* (Tagliaferri et al. 2012a,b), an M-class satellite designed to carry a 2 – 10 keV low-energy polarimeter (LEP) and a 6 – 35 keV medium-energy polarimeter (MEP). To avoid dilution by the GC plasma emission, the MEP is then the most suited instrument to measure polarization from Sgr B2 and Sgr C. The angular resolution (about 20 arcsec) would have been able to spatially resolve the two reflection nebulae, discriminating them from neighborhood sources and potentially enabling the investigation of stratified light echoes from the past activity of Sgr A*.

To calculate the 99 per cent confidence level MDP of the medium/hard X-ray instrument (see Marin et al. 2012b; Strohmayer & Kallman 2013), we derived the flux of Sgr B2 in the MEP band (excluding the iron lines energies where the signal is diluted by unpolarized fluorescence emission) from the 20 – 60 keV energy band (Terrier et al. 2010). The power-law index (Murakami et al. 2000; Sidoli et al. 2001; Terrier et al. 2010) being close to the one of the Crab ($\Gamma \sim 2$), in first approximation we can assume similar fluxes (in mCrab) in the MEP energy band if we neglect absorption below 8 keV. No observation of Sgr C has been made above 10 keV yet, but its soft X-ray continuum has been fitted with a $\Gamma \sim 2$ power law (Murakami et al. 2001; Takagi et al. 2002), similar to Sgr B2. Therefore, we assume for Sgr C a flux in the MEP energy band which is just scaled with respect to that of Sgr B2 by the same factor which is observed in the soft X-rays, that is, a factor 3 fainter (Mu-

Region	P_{source}	MDP	$P_{detect.}$	Error on ψ
Sgr B2	66.5 %	7.7 %	66.7 ± 1.8 %	0.63°
Sgr C	47.8 %	4.5 %	48.7 ± 4.6 %	1.52°

Table 4. Minimum detectable polarization (MDP) of the reflection nebulae with a 500 ks observation with the MEP on board of *MHXM*. Predictions on the detected polarization $P_{detect.}$ and the error on ψ are calculated from Monte Carlo simulations.

rakami et al. 2000). As the count rates from the molecular clouds are faint, we integrate the flux in the largest possible energy range to provide a representative value of the 8 – 35 keV MDP for a 500 ks observation (further details are provided in Marin et al. 2013). Estimations on the detected polarization $P_{detect.}$ and the error on ψ are calculated from Monte Carlo simulations, such as presented in Dovčiak et al. (2011), and are derived from the generation of test modulation curves. The expected initial polarization P_{source} is taken from our modeling of the GC examined in Sect. 2.2.

Results are presented in Tab. 4. We find that both reflecting nebulae are detectable using a 500 ks observation with *NHXM* (MDP $< P_{source}$). Longer exposure time would help to reach lower MDP values and increase the statistic that becomes relevant to measure the polarization angle, but Tab. 4 shows that a medium-sized polarimetric mission would already be able to measure the polarization emerging from Sgr B2 and Sgr C with great precision. Errors on ψ being marginal, the detection of polarization position angle normal to the scattering plane would be unambiguous. Hence, since unpolarized emission from Galactic plasma emission in the soft X-ray band should weaken polarization detection, a mission equipped with a broadband polarimeter is the most suited to provide the cleaner measurement.

3 DISCUSSION

3.1 Additional targets

Our simulations showed that the three-dimensional position of the reprocessing Sgr B2 and Sgr C clouds can be estimated using X-ray polarization measurement above 7 keV. Clouds situated at large distances from the Galactic plane will produce lower polarization degrees as the angle between the source, the scattering medium and the observer will depart from orthogonality. P is thus a function of the position of the emitting source. Targeting a unique reflection nebula will indeed prove or reject the outburst scenario by measuring ψ (Churazov et al. 2002), but it will be necessary to observe at least two nebulae to constrain the three-dimensional location of Sgr A*. From them it will become easier to reconstruct the layout of circumnuclear clouds with respect to the supermassive black hole in the GC. However, Tab. 2 showed that the polarization degree of clouds either at the rear or in front of the Galactic plane decreases as they depart from the plane-of-the-sky. From only two measurements it might be difficult to decide if the clouds are behind or in front of this plane. To break potential degeneracies it will be necessary to measure as many reflection nebulae as possible in order to numerically reconstruct a three-dimensional structure of the GC that coherently reproduces each polarization percentage detected.

The dense environment of the GC provides several other potential targets in which hard X-ray continuum and Fe Kα emission have been found, spatially coincident with GC molecular clouds: Sgr B1 (Koyama et al. 2007), M0.74-0.09 (Koyama et al. 2007), G0.11-0.11 (Ponti et al. 2010), M0.74-0.09 (Nobukawa et al. 2011), M1 (Ponti et al. 2010), M2 (Ponti et al. 2010) or the molecular complex called the Bridge (Guesten & Downes 1980; Bamba et al. 2002). Measuring P and ψ from such a collection of reflection nebulae will help us to determine their location with respect to Sgr A* and test if the central supermassive black hole was the unique, faded illuminating source. One must be cautious though, as some of these scattering clouds present the same characteristic as Sgr B2: a decay of their Fe Kα emission (Koyama et al. 2008; Inui et al. 2009; Terrier et al. 2010). Flux diminution is consistent with the reflection mechanism as light needs time to reach the core of the molecular cloud, facing an increasing molecular density and thus higher absorption probability. Sgr B2 and Sgr C being the brightest sources among the reflection nebulae, they remain the best targets for future X-ray polarization measurement, despite the fact that the duty cycle of the GC accretion activity and the flux of molecular clouds in the next decade (the time frame of a possible mission able to measure the polarization) are an open question. Since the efficiency of a detection relies on the luminosity of the source, the MDP can become too large for several objects, such as Sgr B1 and M0.74-0.09, both fainter than Sgr B2 and also exhibiting temporal decreasing intensity (Koyama et al. 2007).

3.2 Alternative scenario for the origin of X-ray emission from Sgr B2 and Sgr C

X-ray polarimetry can be a powerful tool to examine other scenarios in which the power-law continuum and the 6.4 keV iron feature detected in Sgr B2, Sgr C and other sources, such as the Galactic ridge (Valinia et al. 2000) and G0.13–0.13 (Yusef-Zadeh et al. 2002), are produced by low-energy cosmic-ray electrons rather than by Thomson/Compton scattering (Valinia et al. 2000; Yusef-Zadeh et al. 2002; Dogiel et al. 2009; Yusef-Zadeh et al. 2013). In this model (Valinia et al. 2000; Yusef-Zadeh et al. 2002), nonthermal X-ray emission arises from the interaction of fast electrons ($E < 1$ MeV) with the GC molecular clouds. Emission lines result from the filling of inner-shell vacancies produced by the low-energy cosmic-ray electrons traveling in the atomic mixture while the power-law continuum results from bremsstrahlung processes. Such a mechanism provides fits of similar quality when compared to neutral reflection from a flaring source (Yusef-Zadeh et al. 2002) but polarization can discriminate between the two interpretations.

Bremsstrahlung radiation is generally polarized with its electric vector perpendicular to the plane of interaction. In the case of thermal bremsstrahlung, the planes of interaction are randomly distributed, resulting in null net polarization. Bremsstrahlung emission can be polarized only for an anisotropic distribution of electrons. However, very little is known about the atomic and molecular distribution in the reflection nebulae. Looking at the central 12 pc of the Sgr B2 molecular cloud in the 3 mm band, Jones et

al. (2008) identified at least seven distinct molecular features concentrated at various positions in the cloud complex. The structure of Sgr B2 was previously estimated with $J = 1 \rightarrow 0$ transition of ^{13}CO and C^{18}O by Lis & Goldsmith (1989), who also found a stratification of the cloud, with an increase of ^{13}CO optical depth at the center of the cloud. Hints tend to point toward an asymmetric distribution of matter within the molecular clouds and thus should lead to polarized bremsstrahlung emission, which remains to be estimated.

4 CONCLUSIONS

The simulations undertaken in this paper consolidate the results from the toy-model investigated by Churazov et al. (2002) in the context of a future X-ray polarimetric observations. The $2^\circ \times 2^\circ$ Galactic inner region is expected to be dominated by large polarized fluxes originating from the CND surrounding Sgr A*, with an integrated polarization of the order of 1 per cent. The two main reflection nebulae are identified as the best targets for spatially-resolved X-ray polarization measurement, as they should produce $P \gg 10$ per cent. The degree of polarization from Sgr B2 and Sgr C is a function of the spatial location of these clouds and can constrain the distance of the reflecting nebulae to the central supermassive black hole. Measuring the polarization position angle of Sgr B2 and Sgr C with the GPD instrument at the focus of an X-ray optics would then pinpoint the illuminating source of the molecular clouds and determine if the tentative past flare from Sgr A* is a viable source for the diffuse emission reported by Sunyaev et al. (1993), Koyama et al. (1996) and Murakami et al. (2001). The reconstruction of the light-curve of Sgr A* outburst can be achieved if the detector has a field of view with sufficient enough resolution, such as the concept proposed previously for *NHXM*.

ACKNOWLEDGEMENTS

We thank the anonymous referee for helpful comments. The authors also acknowledge support from the collaboration project between the Czech Science Foundation and Deutsche Forschungsgemeinschaft (GACR-DFG 13-00070J), as well as the COST-CZ LD12010 grant.

REFERENCES

Baganoff, F. K., Bautz, M. W., Brandt, W. N., et al. 2001, Nature, 413, 45
Baganoff, F. K., Maeda, Y., Morris, M., et al. 2003, ApJ, 591, 891
Bally, J., Stark, A. A., Wilson, R. W., & Henkel, C. 1988, ApJ, 324, 223
Bamba, A., Murakami, H., Senda, A., et al. 2002, ESTEC, The Netherlands, ESA SP-488
Barrière, N. M., Tomsick, J. A., Baganoff, F. K., et al. 2014, arXiv:1403.0900
Bélanger, G., Goldwurm, A., Melia, F., et al. 2005, ApJ, 635, 1095
Clavel, M., Terrier, R., Goldwurm, A., et al. 2013, A&A, 558, A32
Christopher, M. H., Scoville, N. Z., Stolovy, S. R., & Yun, M. S. 2005, ApJ, 622, 346
Churazov, E., Sunyaev, R., & Sazonov, S. 2002, MNRAS, 330, 817
Costa, E., Soffitta, P., Bellazzini, R., et al. 2001, Nature, 411, 662
Dogiel, V., Cheng, K.-S., Chernyshov, D., et al. 2009, PASJ, 61, 901
Dovčiak, M., Muleri, F., Goosmann, R. W., Karas, V., & Matt, G. 2011, ApJ, 731, 75
Eckart, A., Schödel, R., Baganoff, F. K., et al. 2008, Journal of Physics Conference Series, 131, 012002
Ghez, A. M., Salim, S., Weinberg, N. N., et al. 2008, ApJ, 689, 1044
Gillessen, S., Eisenhauer, F., Fritz, T. K., et al. 2009, ApJL, 707, L114
Goosmann, R. W., & Gaskell, C. M. 2007, A&A, 465, 129
Goosmann, R. W. 2010, X-ray Polarimetry: A New Window in Astrophysics by Ronaldo Bellazzini, Enrico Costa, Giorgio Matt and Gianpiero Tagliaferri. Cambridge University Press, 2010. ISBN: 9780521191845, p. 136, 136
Guesten, R., & Downes, D. 1980, A&A, 87, 6
Heiligman, G. M. 1987, ApJ, 314, 747
Inui, T., Koyama, K., Matsumoto, H., & Tsuru, T. G. 2009, PASJ, 61, 241
Jones, P. A., Burton, M. G., Cunningham, M. R., et al. 2008, MNRAS, 386, 117
Kendrew, S., Ginsburg, A., Johnston, K., et al. 2013, ApJL, 775, L50
Koyama, K., Makishima, K., Tanaka, Y., & Tsunemi, H. 1986, PASJ, 38, 121
Koyama, K., Awaki, H., Kunieda, H., Takano, S., & Tawara, Y. 1989, Nature, 339, 603
Koyama, K., Maeda, Y., Sonobe, T., et al. 1996, PASJ, 48, 249
Koyama, K., Inui, T., Hyodo, Y., et al. 2007, PASJ, 59, 221
Koyama, K., Inui, T., Matsumoto, H., & Tsuru, T. G. 2008, PASJ, 60, 201
Law, C. J., Yusef-Zadeh, F., Cotton, W. D., & Maddalena, R. J. 2008, ApJS, 177, 255
Liedahl, D. A. 1999, X-Ray Spectroscopy in Astrophysics, 520, 189
Lis, D. C., & Goldsmith, P. F. 1989, ApJ, 337, 704
Liu H. B.; Ho P. T. P.; Wright M. C. H.; Su Y.; Hsieh P.; Sun A.; Kim S. S.; and Minh Y. C. 2014, arXiv:1402.1005
Marin, F., Goosmann, R. W., Gaskell, C. M., Porquet, D., & Dovčiak, M. 2012a, A&A, 548, A121
Marin, F., Goosmann, R. W., Dovčiak, M., et al. 2012, MNRAS, 426, L101
Marin, F., Porquet, D., Goosmann, R. W., et al. 2013, MNRAS, 436, 1615
Mewe, R. 1999, Edited by Jan van Paradijs and Johan A. M. Bleeker. Lecture Notes in Physics, Vol. 520, Springer, 1999., p.109
Mills, E. A. C., Güsten, R., Requena-Torres, M. A., & Morris, M. R. 2013, ApJ, 779, 47
Molinari, S., Swinyard, B., Bally, J., et al. 2010, PASP, 122, 314
Molinari, S., Bally, J., Noriega-Crespo, A., et al. 2011, ApJL, 735, L33
Morris, M., Polish, N., Zuckerman, B., & Kaifu, N. 1983, AJ, 88, 1228

Murakami, H., Koyama, K., Sakano, M., Tsujimoto, M., & Maeda, Y. 2000, ApJ, 534, 283
Murakami, H., Koyama, K., Tsujimoto, M., Maeda, Y., & Sakano, M. 2001, APJ, 550, 297
Neilsen, J., Nowak, M. A., Gammie, C., et al. 2013, ApJ, 774, 42
Nobukawa, M., Ryu, S. G., Tsuru, T. G., & Koyama, K. 2011, ApJL, 739, L52
Ponti, G., Terrier, R., Goldwurm, A., Belanger, G., & Trap, G. 2010, ApJ, 714, 732
Ponti, G., Morris, M. R., Terrier, R., & Goldwurm, A. 2013, Cosmic Rays in Star-Forming Environments, Astrophysics and Space Science Proceedings, Vol. 34. ISBN 978-3-642-35409-0. Springer-Verlag Berlin Heidelberg, 2013, p. 331
Porquet, D., Predehl, P., Aschenbach, B., et al. 2003, A&A, 407, L17
Quataert, E. 2002, ApJ, 575, 855
Reid, M. J., Menten, K. M., Zheng, X. W., et al. 2009, ApJ, 700, 137
Ryu, S. G., Nobukawa, M., Nakashima, S., et al. 2013, PASJ, 65, 33
Sidoli, L., & Mereghetti, S. 1999, A&A, 349, L49
Sidoli, L., Mereghetti, S., Treves, A., et al. 2001, A&A, 372, 651
Soffitta, P., Barcons, X., Bellazzini, R., et al. 2013, Experimental Astronomy, 36, 523
Strohmayer, T. E., & Kallman, T. R. 2013, ApJ, 773, 103
Sunyaev, R. A., Churazov, E. M., Gil'Fanov, M. R., et al. 1991, Advances in Space Research, 11, 177
Sunyaev, R. A., Markevitch, M., & Pavlinsky, M. 1993, ApJ, 407, 606
Sunyaev, R., & Churazov, E. 1998, MNRAS, 297, 1279
Takagi, S.-i., Murakami, H., & Koyama, K. 2002, ApJ, 573, 275
Tagliaferri, G., Hornstrup, A., Huovelin, J., et al. 2012a, Experimental Astronomy, 34, 463
Tagliaferri, G., & NHXM consortium, o. b. o. t. 2012b, MemSAI, 83, 360
Terrier, R., Ponti, G., Bélanger, G., et al. 2010, ApJ, 719, 143
Tsuboi, M., Handa, T., & Ukita, N. 1999, ApJS, 120, 1
Valinia, A., Tatischeff, V., Arnaud, K., Ebisawa, K., & Ramaty, R. 2000, ApJ, 543, 733
Weisskopf, M. C., Silver, E. H., Kestenbaum, H. L., Long, K. S., & Novick, R. 1978, ApJL, 220, L117
Yusef-Zadeh, F., Law, C., & Wardle, M. 2002, ApJL, 568, L121
Yusef-Zadeh, F., Braatz, J., Wardle, M., & Roberts, D. 2008, ApJL, 683, L147
Yusef-Zadeh, F., Hewitt, J. W., Arendt, R. G., et al. 2009, ApJ, 702, 178
Yusef-Zadeh, F., Hewitt, J. W., Wardle, M., et al. 2013, ApJ, 762, 33

This paper has been typeset from a TEX/ LATEX file prepared by the author.